Nanochem Res 6(2): 239-247, Summer and Autumn 2021

RESEARCH PAPER

In-situ Additive Engineering of PbI_2 Framework by Dopamine for Improving Performance of Mesostructure $CH_3NH_3PbI_3$ Solar Cells

Hojjat Amrollahi Bioki[1], Ahmad Moshaii[1,*], Mahmoud Borhani Zarandi[2]

[1] *Department of Physics, Tarbiat Modares University, Tehran, Iran*

[2] *Department of Physics, Yazd University, Yazd, Iran*

ARTICLE INFO

Article History:
Received 28 June 2021
Accepted 03 September 2021
Published 15 October 2021

Keywords:
Dopamine hydrochloride
Efficiency
Grain size
Organic ligand additive
Perovskite solar cells

ABSTRACT

Additive-assisted interfacial engineering is a strategy to enhance the performance of perovskite solar cells (PSCs). A high-quality perovskite active layer, with defect-free, plays a key role in the performance of the solar cells. Herein, a dopamine hydrochloride (DA), as an organic ligand, was incorporated into the $CH_3NH_3PbI_3$ perovskite precursor solution for modifying the microstructure of perovskite films and the photovoltaic properties of the PSCs. The result of the study indicated that the DA additive in perovskite precursor is a promising strategy for obtaining compact and uniform $CH_3NH_3PbI_3$ film, which can effectively reduce the recombination of charge carriers. The PSCs modified by the DA additive exhibited enhanced photovoltaic performance compared to the PSCs without modification. Optimum power conversion efficiency (PCE) of the PSCs significantly improved (13.57%) compared to that of the device without modification (10.22%). In addition, the PSCs with a 0.6 wt% DA in the perovskite precursor showed a satisfactory fabrication producibility compared to the pristine one. Therefore, this work presents a simple and effective way to develop reproducible and efficient PSCs by DA treatment.

How to cite this article
Amrollahi Bioki H., Moshaii A., Borhani Zarandi M. In-situ Additive Engineering of PbI_2 Framework by Dopamine for Improving Performance of Mesostructure $CH_3NH_3PbI_3$ Solar Cells. Nanochem Res, 2021; 6(2):239-247. DOI: 10.22036/ncr.2021.02.010

INTRODUCTION

Organic-inorganic hybrid perovskite materials have received much attention due to their high absorption coefficient, bipolar transmission, long carrier lifetime, low-cost raw materials, and simple preparation processes. The perovskite solar cell (PSC) is one of the third-generation photovoltaic technologies which are considered most likely to be industrialized in the future. So far, the photoelectric conversion efficiency (PCE) of the perovskite solar cells has reached 25.5% within the past few years, and this increase is attributed to composition engineering, processing improvement, and architecture optimization [1, 2]. The photovoltaic properties of the PSCs practically depend on the compositions and crystal structures of the perovskite compounds. The perovskite films with high crystallinity, few grain boundary defects, and dense and uniform films can effectively reduce the recombination of charge carriers at the crystal or grain boundary, improve the mobility of carriers, and enhance the photovoltaic performance of the solar cell [3, 4]. A large number of reports exist on the modification of the perovskite layer and its interface for improving its crystallinity and optimizing the interface energy level matching with the perovskite so that the performance of the solar cell can improve [5, 6]. Further, additive engineering on the perovskite precursor solution has proven to be an effective approach in forming a high-quality perovskite film. The hydrogen bonding or coordination between the additive and perovskite components can slow down the crystallization rate of the perovskite

* Corresponding Author Email: *moshaii@modares.ac.ir*

This work is licensed under the Creative Commons Attribution 4.0 International License.
To view a copy of this license, visit http://creativecommons.org/licenses/by/4.0/.

crystals in solution processing to achieve large crystal grains and thereby improve PCE, since the lead and iodide ions in the perovskite have good coordination ability [7]. Various additives have been reported for adjusting the morphology of the perovskite films such as ionic liquid, polar aprotic solvents including dimethyl sulfoxide (DMSO) and dimethyl formamide (DMF), organic groups of ligands as Lewis bases, and metal-organic frameworks (MOF) as molecular additives [8-11]. The operation mechanism of these additives is mainly based on the cross-link or chelating effect between the perovskite grains and functional groups, such as hydroxyl group (-OH), carboxyl group (-COOH), and ammonium group ($-NH_2$), which commonly interact with Pb^{2+} or I^- ions and change the perovskite crystallization [12].

Organic additives are the most common types of additives used in PSCs. These organic additives can be further categorized based on N, O, and S donor atoms. These electron donor atoms can bind/coordinate with the Pb^{2+} species, leading to adduct formation, passivating the grain boundaries, and, thus, resulting in a slow crystallization process to grow large PbI_2 flakes [13]. However, few studies have applied Lewis bases in the two-step solution process on perovskite film formation for modulating the morphology of perovskite films. Although the reaction between methylammonium iodide (MAI) and PbI_2 is almost instantaneous in the two-step method [14], the effect of the additive for the two-step processing signifies the perovskite formation. It is well-known that the two-step process prefers nucleation of MAI at the PbI_2 grain boundaries and defects, and PbI_2 flakes with larger grain sizes can decrease boundary defects, leading to fewer nucleation sites of perovskites. This means that the morphology of PbI_2 plays a critical role in determining the final morphology of a perovskite layer including its crystallization, grain size, and uniform surface coverage [15].

In this study, we demonstrate a novel strategy for making porous metal–organic structures of PbI_2 crystals, involving in-situ coordination assembly of Pb ions with dopamine hydrochloride (DA) as an organic ligand. Adding DA into the PbI_2 solution results in releasing organic ligand molecules and creating hollow structures in the formation of the perovskite $CH_3NH_3PbI_3$ film during two-step processing. The mesoporous TiO_2-based PSCs were fabricated to study the effects of DA additive on photovoltaic properties of PSCs. To the best of our knowledge, this is the first report to add Lewis base into the PbI_2 soaking solution.

EXPRIMENTAL METHODS

Materials

Fluorine-doped tin oxide (FTO, 8 Ω/sq) and methylammonium iodide (CH_3NH_3I, MAI) were provided by Dyesol Ltd. Lead iodide (PbI_2), copper(II) phthalocyanine ($C_{32}H_{16}CuN_8$,CuPc), dopamine hydrochloride ($C_8H_{11}NO_2$), *N*,*N*-dimethyl formamide (DMF), dimethyl sulfoxide (DMSO), isopropyl alcohol (IPA), titanium(IV) tetra isopropoxide (TTIP), and all of the additional chemicals were obtained from Sigma-Aldrich.

Solar cell fabrication

The FTO glass substrate (2.5 cm×2.5 cm) was ultrasonically cleaned with detergent, acetone, ethanol, and deionized water for 15 minutes each, and finally processed in an ultraviolet ozone cleaning chamber for 20 min. To deposit the electron-transporting layer (ETL), the TTIP sol in ethanol (containing 1.0 M HCl) was dropped onto the processed FTO glass substrate, spin-coated at 3000 rpm for 30 s, and then sintered in a furnace at 500 °C for 30 min to obtain a compact layer of TiO_2 (c-TiO_2). The TiO_2 paste (18NR-T, Sharif Solar, particle size ~20 nm), diluted to 20 wt% with ethanol, was spin-coated on the c-TiO_2 layer at 4000 rpm for 30 s, and then sintered at 500 °C for 30 min to obtain a titanium dioxide mesoporous (mp-TiO_2) layer substrate.

We also applied two-step sequential spin-coating technique for preparing the $MAPbI_3$ perovskite layer. DA as an additive was used in the PbI_2 solution, since PbI_2 is a proper precursor for fabricating efficient lead iodide perovskite structures . First, 462 mg PbI_2 was dissolved in anhydrous DMF:DMSO (950:50 µl) at 70 °C to obtain a 1.0 M solution with different DA content (0, 0.2, 0.4, 0.6, and 0.8 wt%). The PbI_2 solutions were spin-coated on the mp-TiO_2 layer at 3000 rpm for 30 s. Then, the resulting wet film was heat-treated at 90 °C for 10 min and the 40 mg/ml solution of MAI in IPA at 80 °C was immediately dropped on it and kept for 20 s, and then spin-coated at 2500 rpm for 30 s. The film was annealed at 100 °C for 10 min to form a dark perovskite layer. All of the processes were conducted outside the glove-box environment.

CuPc (50 nm) was deposited by thermal evaporation onto the formed $CH_3NH_3PbI_3$

CC BY

perovskite under the pressure of 5×10^{-5} mbar to deposit the hole-transporting layer (HTL). Furthermore, 100 nm of Ag was deposited by thermal evaporation to complete the device. The active area of the cells made in this work is about 0.08 cm^2.

Characterizations

The surface morphology of the films was characterized by scanning electron microscopy (SEM, TESCAN, VEGA3). Optical absorption was recorded by UV-visible spectroscopy (Ocean Optics, HR 4000), and the steady-state photoluminescence (PL) spectra were measured with Varian Cary Eclipse Fluorescence spectrometer. Additionally, the photo current-voltage (I-V) characteristic curve was measured by a Keithley 2400 potentiostat under a calibrated AM 1.5G (100 mW/cm^2) simulated solar light source. The short-circuit current density (J_{sc}), open-circuit voltage (V_{oc}), fill factor ($FF=P_{max}/(J_{sc}\times V_{oc})\times100\%$), and photoelectric conversion efficiency (PCE = $J_{sc}\times V_{oc}\times FF$) were calculated by using the J-V characteristic curve of fabricated solar cells [16]. Moreover, the incident photon-current conversion efficiency (IPCE) spectrum of solar cells was measured by applying the IPCE system (Sharif Solar IPCE-020). The electrochemical impedance spectroscopy (EIS) of the PSCs were characterized by using potentiostat/galvanostat (PGSTAT 30, Autolab, Eco-Chemie) under dark conditions with the measured frequency ranging from 1 Hz to 1 MHz. All of analyses and other processes were carried out in air environment with a relative humidity (RH) of ≈ 30 % without any encapsulation.

RESULTS AND DISCUSSION

SEM analysis

The effect of the DA additive on the surface morphology of the PbI_2 film and corresponding perovskite film were investigated by SEM, as shown in Fig. 1 and 2, respectively. The deposition of PbI_2 films with or without DA additive is shown schematically in Fig. 1(a). The SEM micrographs of PbI_2 thin films and their distribution histogram of grain sizes with different content of DA additive in PbI_2 procedure are shown in Fig. 1(b-f). It can be inferred that the PbI_2 film without DA is relatively compact with the average aggregated grain size of about 280 nm (Fig. 1b), and as the concentration of DA increases, a large number of pores on the reverse side of the PbI_2 film gradually appear. In addition, the PbI_2 films with the average uniform grain size of 270 nm were obtained when the content of DA is 0.6 wt% (Fig. 1e). This porosity is conducive to the subsequent penetration of the MAI/IPA solution and better reaction with the PbI_2 film, thereby resulting in forming a highly oriented perovskite films.

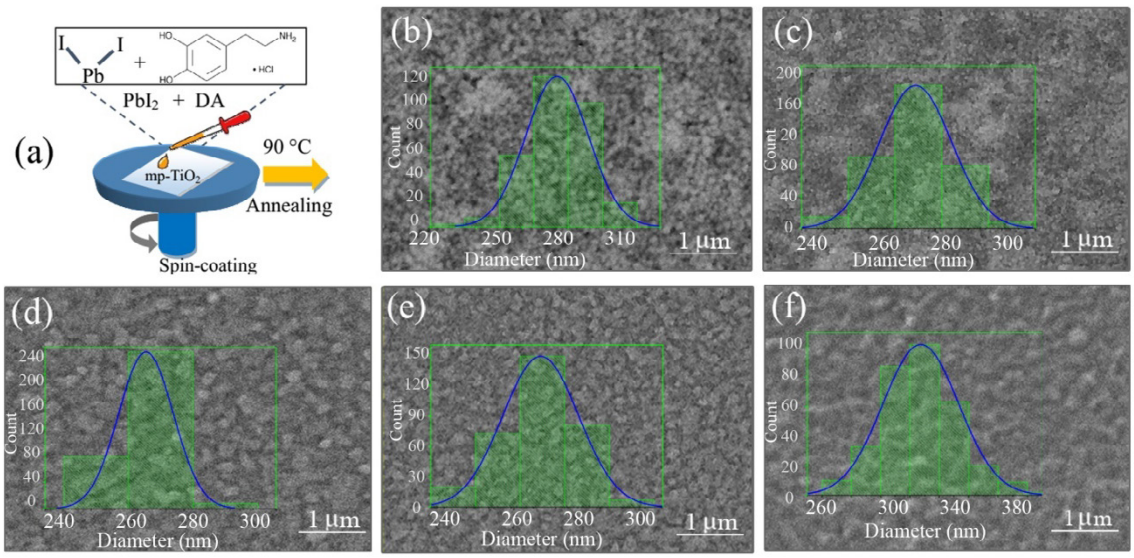

Fig. 1. (a) Schematic procedure for the preparation of PbI_2 film with DA additive. Surface SEM images with histogram of particle size for PbI_2 films deposited on the mp-TiO_2 with or without DA linker in PbI_2 procedure; (b) without DA; (c) 0.2 wt% DA; (d) 0.4 wt% DA; (e) 0.6 wt% DA; (f) 0.8wt% DA

CC BY

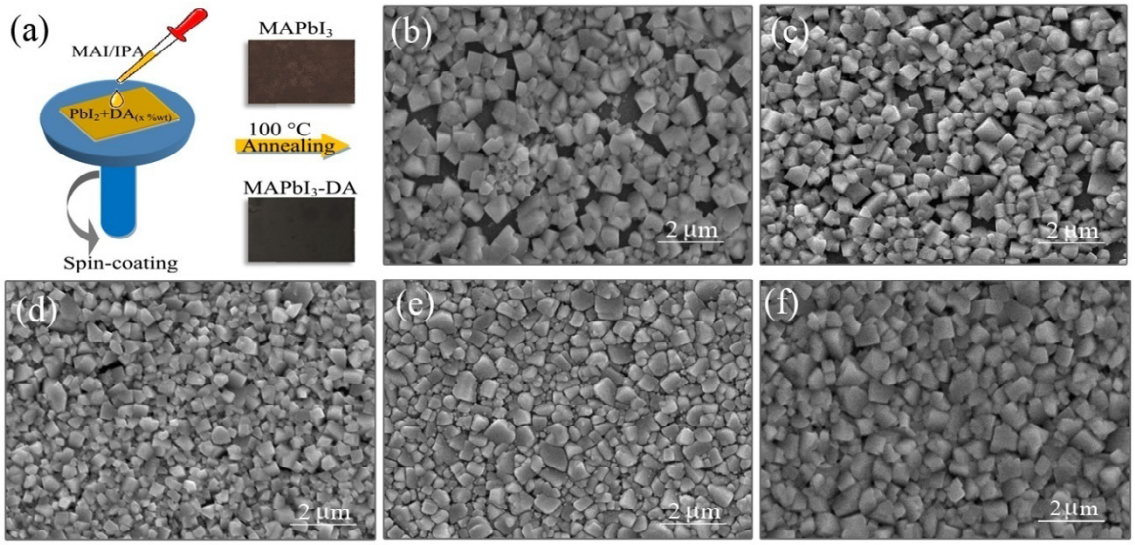

Fig. 2. (a) Schematic of preparation of $MAPbI_3$ by spin-coating MAI solution on PbI_2 film with DA additive. Surface SEM images of perovskite films with various concentration of DA in PbI_2 precursor (a) without DA; (b) 0.2 wt% DA; (c) 0.4 wt% DA; (d) 0.6 wt% DA and (e) 0.8 wt% DA.

The schematics of MAI deposition on PbI_2-DA by spin-coating to form the perovskite layer are shown in Fig. 2 (a). The SEM micrographs of the perovskite layer reveal that after the DA treatment, the pin-holes and grain boundary defects disappeared (Fig. 2b), and the PbI_2 film modified by 0.6 wt% DA makes a framework substrate to produce uniform, continuous, and compact perovskite films (Fig. 2e). In addition, when the MAI solution spin-coated on the PbI_2-DA substrate, the color of PbI_2 film changed during the 10 s after spinning started, which was much faster than the conversion of the pure PbI_2 films (>25 s). This faster change of color indicates a rapid diffusion of MAI in the PbI_2 framework which initiates a faster perovskite reaction, thus creating a condition which is favorable for the growth of large $MAPbI_3$ perovskite crystals (Fig 2c-f). This phenomenon could be attributed to the formation of hydrogen bonds among the $-NH^{3+}$ groups of the DA and the halide anions of the perovskite, resulting in increasing the growth activation energy during the formation of perovskite films, which is beneficial for preparing the perovskite films of higher crystallinity as demonstrated by Hou et al. reports [17].

The pinholes and grain boundaries provide channels for defusing water and oxygen from the environment into the perovskite layer, which impairs the long-term stability and solar cells performance [18].

Optical properties

The UV-Vis absorption spectra of the PbI_2 thin films with different DA content on mp-TiO_2 coated FTO substrates and the corresponding $MAPbI_3$ films are shown in Fig. 3(a) and 3(b), respectively. Based on Fig. 3(a), with increasing DA content, the absorbance in PbI_2 film increases and the maximum absorbance occurs with 0.6 wt% DA, confirming the formation of PbI_2-framework crystals [19]. The low absorbance in pure PbI_2 is mainly due to the small crystal size of PbI_2, leading to lower contribution to light scattering.

It can be seen from Fig. 3b that with increasing the DA content (such as the sample with 0.6 wt% DA added into PbI_2 films), the absorption of the perovskite film gradually increases, especially in the wavelength region of 380 to 780 nm. This increase is mainly due to the larger grain size and relatively dense perovskite film. As the deposited PbI_2 thin film and corresponding prepared $MAPbI_3$ absorption spectra indicate, their absorption cut-off wavelengths are about 505 nm and 755 nm, respectively (Fig .3). This result reveals that the perovskite thin films can absorb visible light in the wavelength region of 460–790 nm. The cut-off wavelength can be used to calculate the optical bandgap of the film by using $E_g=hc/\lambda_c$, where E_g represents optical bandgap, h denotes Planck's

CC BY

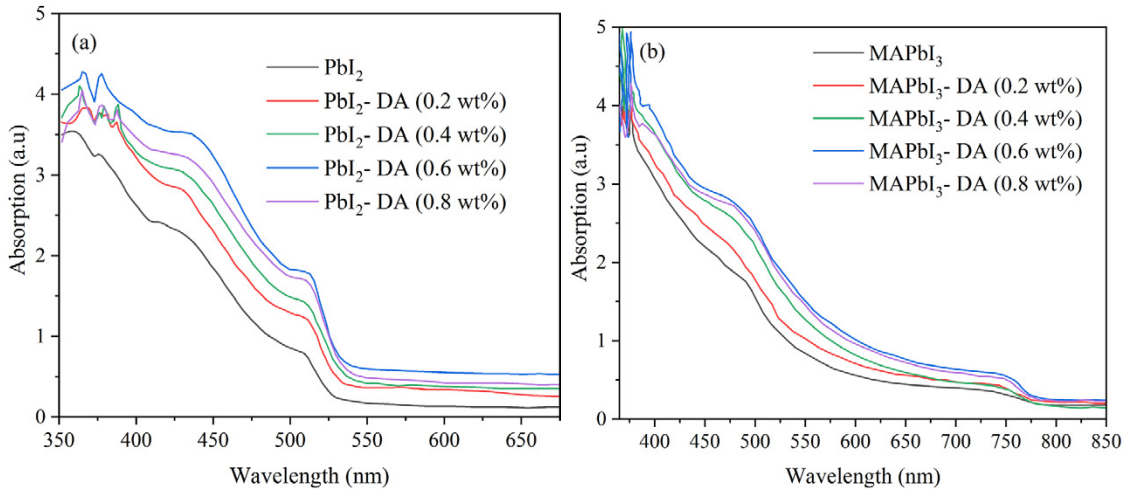

Fig. 3. UV-Visible absorption spectra of (a) PbI_2 films and (b) corresponding $MAPbI_3$ in presence of various concentration of DA.

Table 1. Optical bandgap for PbI_2 films with different additive contents of DA and their corresponding perovskite layer.

DA content in samples		0 wt%	0.2 %wt	0.4 wt%	0.6 wt%	0.8 wt%
Bandgap (eV)	PbI_2	2.34	2.30	2.28	2.26	2.26
	$MAPbI_3$	1.68	1.66	1.65	1.62	1.63

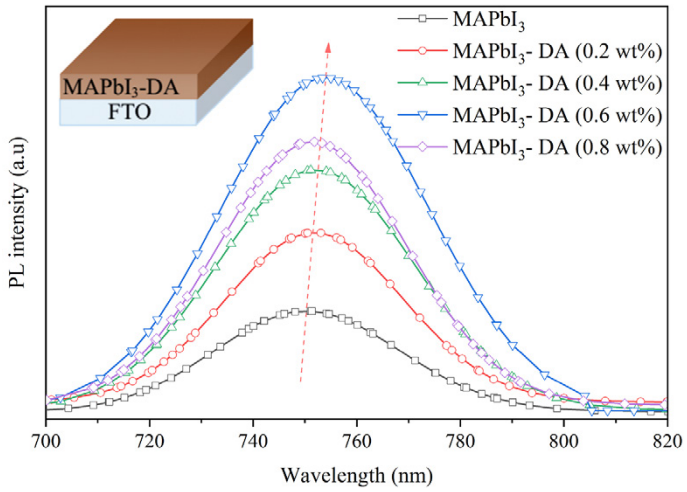

Fig. 4. Steady state photoluminescence (PL) spectra of $MAPbI_3$ films doped with various concentrations of DA deposited on top of FTO

constant, *c* stands for the speed of light, and λ_c is the cut-off wavelength [20]. The optical bandgap for PbI_2 films and its corresponding perovskite layer are given in Table 1. It can be seen that the bandgap of $MAPbI_3$ reduces from 1.68 to 1.62 eV when the DA content in PbI_2 increases from 0 to 0.6 wt%. This result shows that the control of the DA content in PbI_2 is crucial for obtaining certain optical bandgap value of the perovskite film. The value of optical bandgap will affect the light harvesting and selection of hole and electron transport layers for enhancing charge transport in the cells, and hence improving the PCE of the cells.

In order to compare the effect of DA additive on the defect state and crystallinity of the perovskite film, we studied the PL spectra of the perovskite film under excitation laser pulse at 480 nm. Fig. 4 shows the PL spectra of perovskite films (deposited

on top of FTO) with different concentrations of DA additive. We can conclude that the strongest PL intensity for all samples is around 770 nm, which is consistent with the starting point of the absorption edge of the UV-Vis absorption spectrum (Fig. 3b). In addition, Fig. 4 indicates that the perovskite films with DA additive have higher PL intensity compared with the pristine perovskite film, which is attributed to the higher crystallinity and less defect states of the film. Further, the Stokes-shift in PL emission peak and absorption edge of $MAPbI_3$ films with DA additive is relatively small; however,

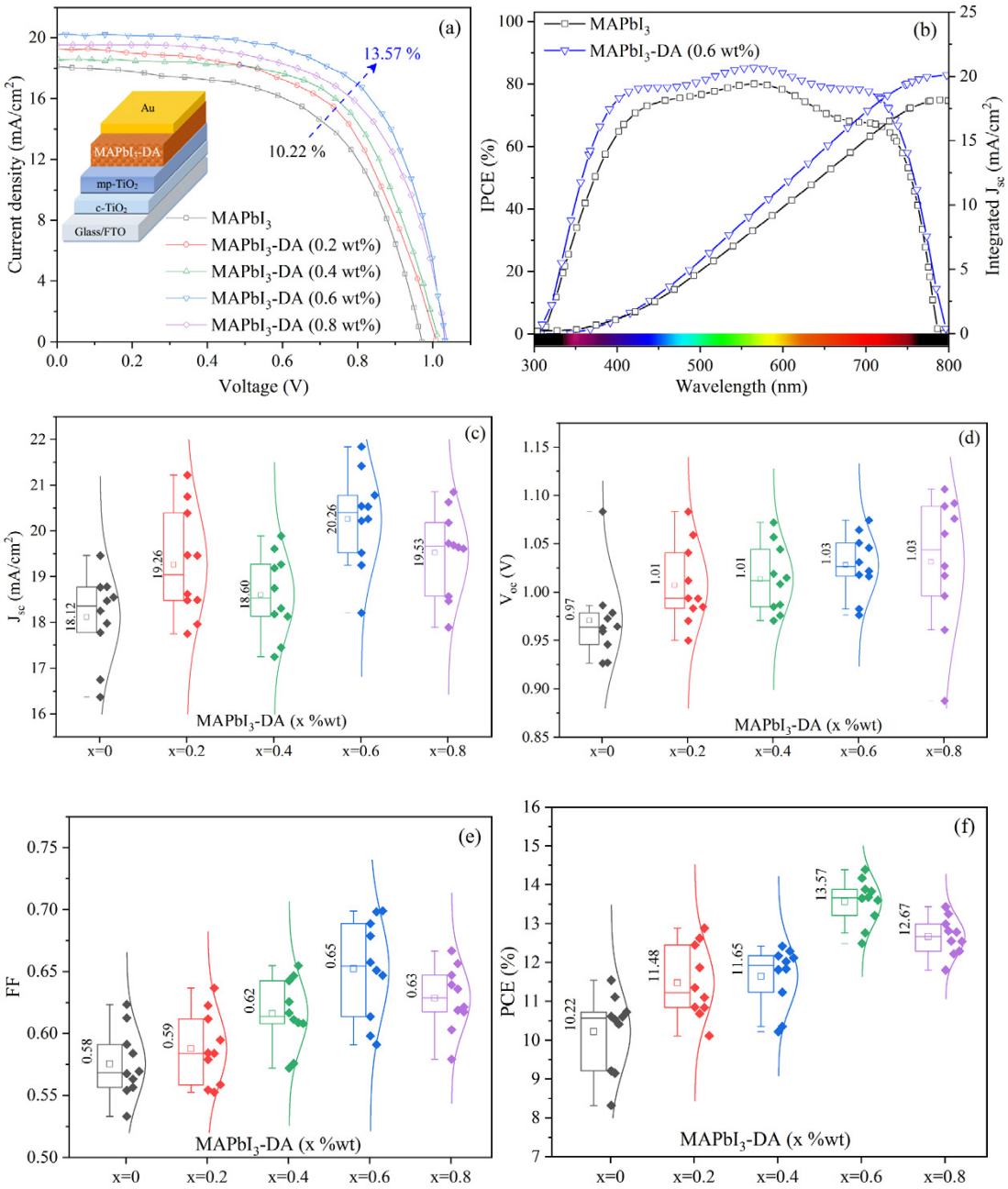

Fig. 5. (a) Averaged J-*V* curves of the PSCs with various concentrations of DA under illumination; (b) IPCE spectrum of the PSCs fabricated from precursor solution added with 0.4 wt% DA and the integration photocurrent curves of the PSCs; Statistical distribution and box-plots of photovoltaic parameters (c) J_{sc}, (d) V_{oc}, (e) FF, (f) PCE of a series of PSCs obtained from J–V curves under illumination.

CC BY

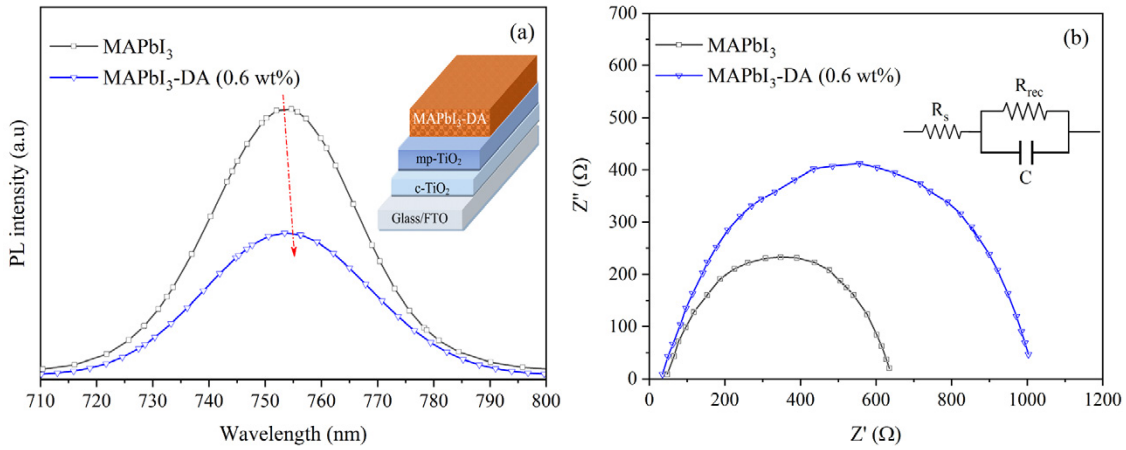

Fig. 6. (a) Steady-state PL spectra of $MAPbI_3$ without or with 0.6 wt% DA. Inset: The photoanode composed of $MAPbI_3$/ETL layers. (b) Nyquist plots of the PSCs without or with 0.6 wt% DA. Inset: The equivalent circuit model for fitting the plots.

the PL intensity is significantly high when the amount of DA reaches 0.6 wt%, which may result from the crystallization dynamics [21].

PSCs performance analysis

To further verify the general applicability of DA in PSCs, the current density-voltage (J-V) curve of the PSCs with different content of DA in PbI_2 procedure is shown in Fig. 5(a). The results show that the PSCs fabricated with DA additive have better photovoltaic performances than those from the pristine PSCs. The devices with 0.6 wt% DA treatment exhibited the best PCE (13.57%), which is higher than that of the pristine device (10.22%).

The statistic results for the PSC parameters fabricated from different content of DA in PbI_2 precursor exhibit a similar tendency for ten individual devices as shown in Fig. 5 (c–f). Furthermore, the statistical distribution of PCE reveals better reproducibility for all devices fabricated from the PbI_2 solution with DA additive than those from the solution without DA.

By analyzing the performance parameters of PSCs with different contents of DA (Fig. 5c-f), we can concluded that as the added content of DA increases from 0 to 0.6 wt%, the short-circuit current (J_{sc}) of the PSCs rises from 18.12 to 20.26 $mA{\cdot}cm^{-2}$; the open circuit voltage (V_{oc}) gradually increases from 0.97 to 1.03 V, and then remains basically unchanged; the fill factor (FF) gradually increases from 0.58 to 0.65. First, by increasing DA content to 0.8 wt%, the efficiency gradually increases from 10.22 to 13.57%, and then steadily decreases to 12.67%. This indicates that after adding DA, the carrier recombination phenomenon in the perovskite film gradually decreases, resulting in increasing FF, V_{oc}, J_{sc}, and accordingly the PCE of PSCs.

Figure 5(b) compares the incident photon-to-current efficiency (IPCE) results of a PSC fabricated from PbI_2 solution with/without adding 0.6 wt% DA, which exhibits a good quantum yield. The integrated current density obtained from the IPCE result of the device is basically matched well with the J_{sc} obtained from the J-V curve of PSCs. This indicates the reliability of the photovoltaic parameters measured in this experiment.

The steady-state PL spectra of the $MAPbI_3$ films without or with 0.6 wt% DA deposited on mp-TiO_2 substrate was conducted to evaluate the film defects and related interface charge transfer process between the DA treated perovskite layer and the mp-TiO_2 ETL (see Fig. 6a). It is found by comparison that the intensity of the PL spectra for the $MAPbI_3$:DA is significantly weaker than that obtained for the pure $MAPbI_3$, indicating that the photogenerated electrons on the perovskite are transferred effectively into ETL before they are recombined at the perovskite/ETL interface. Therefore, adding DA in $MAPbI_3$ perovskite film may lead to higher carrier extraction efficiency and fewer carrier recombination, and ultimately result in improving the photovoltaic performance. This improvement in performance is in agreement with the conclusion in Zhang et al. report [18] that the DA modification can help reduce the trap-state

CC BY

density of the perovskite film, thereby contributing to satisfactory device performance.

Small series resistance consisting of the contact resistance, wire resistance, sheet resistance of the electrode, and charge transfer resistance can be advantageous for fabricating high-quality PSCs. The recombination and interface dynamics of charge transfer in the PSCs is revealed by electrochemical impedance spectroscopy (EIS) measurements at a forward bias voltage of 1.0 V under dark conditions. Figure 6(b) shows the Nyquist impedance spectrum corresponding to PSCs without or with 0.6 wt% DA as well as their simulated fits from the equivalent RC circuit model [22] as shown in the inset of Fig. 6(b).

The starting point associated with the main semicircle in the high frequency range represents the series resistance (R_s) of the device. Additionally, the arc of the curve is determined by the heterojunction capacitance (C) and recombination resistance (R_{rec}) counting for the carrier recombination in the interface between the perovskite and the ETL or FTO layer. The radius of the arc represents the resistance value of the R_{rec} [23, 24].

The PSCs based on the DA additive in perovskite precursor shows higher R_{rec} and lower R_s than the PSCs without the DA additive. The R_s value of the PSCs reduces from 47.2 to 34.6 Ω, and the R_{rec} increases from 580 to 962 Ω by adding 0.6 wt% DA in the PbI_2 precursor compared to the pristine one. The small R_s promotes carrier transport, which leads to a high J_{sc} and the high R_{rec} effectively suppresses the charge recombination for improved device performance. A lower value of R_s is expected for PSCs based $MAPbI_3$:DA additive as they exhibit larger grain sizes (Fig. 2c) that could reduce the resistance offered by grain boundaries. Thus, the less charge recombination is mainly attributed to the reduced defect density, which is due to the high quality of the perovskite film [25].

CONCLUSION

In this work, we developed a simple strategy for adding DA into the perovskite precursor solution. In the process of preparing $MAPbI_3$ perovskite film by a two-step method, an appropriate amount of organic ligand of DA was introduced into the PbI_2 precursor solution as an additive to control the crystallization process of the perovskite film and passivate uncoordinated Pb^{2+} defects via Lewis acid-base interactions. Hence, the IPCE, UV-Vis absorption, PL, and EIS characterizations show the passivation effect and an effective reduction in the process of interface charge recombination. The 0.6 wt% DA-mediated PbI_2 solution assisted the growth of perovskite film and led to an appreciable enhancement in both photovoltaic performance and reproducibility of PSCs in comparison with the pristine perovskite. Consequently, the DA additive enhanced the device efficiency up to 13.5%, which is superior to those of the pristine devices. In brief, DA additive in the PbI_2 precursor solution can be applied to construct other perovskite-based hybrid optoelectronic devices.

CONFLICT OF INTEREST

The authors declare that there are no conflicts of interest.

REFERENCES

[1] Yoo JJ, Seo G, Chua MR, Park TG, Lu Y, Rotermund F, et al. Efficient perovskite solar cells via improved carrier management. Nature. 2021;590(7847):587-93.
[2] NREL Best Research Cell Efficiency Chart June 2021. Available from: https://www.nrel.gov/pv/cell-efficiency.html.
[3] Chen J, Kim S-G, Ren X, Jung HS, Park N-G. Effect of bidentate and tridentate additives on the photovoltaic performance and stability of perovskite solar cells. Journal of Materials Chemistry A. 2019;7(9):4977-87.
[4] Yang Y, Peng H, Liu C, Arain Z, Ding Y, Ma S, et al. Bi-functional additive engineering for high-performance perovskite solar cells with reduced trap density. Journal of Materials Chemistry A. 2019;7(11):6450-8.
[5] Zhang Y-N, Li B, Fu L, Zou Y, Li Q, Yin L-W. Enhanced optical absorption and efficient cascade electron extraction based on energy band alignment double absorbers perovskite solar cells. Solar Energy Materials and Solar Cells. 2019;194:168-76.
[6] Huang L, Zhang D, Bu S, Peng R, Wei Q, Ge Z. Synergistic Interface Energy Band Alignment Optimization and Defect Passivation toward Efficient and Simple-Structured Perovskite Solar Cell. Advanced Science. 2020;7(6):1902656.
[7] Kim J, Ho-Baillie A, Huang S. Review of Novel Passivation Techniques for Efficient and Stable Perovskite Solar Cells. Solar RRL. 2019;3(4):1800302.
[8] Johansson MB, Xie L, Kim BJ, Thyr J, Kandra T, Johansson EMJ, et al. Highly crystalline $MAPbI_3$ perovskite grain formation by irreversible poor-solvent diffusion aggregation, for efficient solar cell fabrication. Nano Energy. 2020;78:105346.
[9] Chang T-H, Kung C-W, Chen H-W, Huang T-Y, Kao S-Y, Lu H-C, et al. Planar Heterojunction Perovskite Solar Cells Incorporating Metal-Organic Framework Nanocrystals. Advanced Materials. 2015;27(44):7229-35.
[10] Chen B, Rudd PN, Yang S, Yuan Y, Huang J. Imperfections and their passivation in halide perovskite solar cells. Chemical Society Reviews. 2019;48(14):3842-67.
[11] Ren J, Wang Q, Ji X, Peng X, Xiao Z, Wu Y, et al. Enhancing the performance of mixed-halide perovskite-based light-emitting devices by organic additive inclusion. Synthetic

CC BY

Metals. 2019;253:88-93.
[12] Wang L, Fan B, Zheng B, Yang Z, Yin P, Huo L. Organic functional materials: recent advances in all-inorganic perovskite solar cells. Sustainable Energy & Fuels. 2020;4(5):2134-48.
[13] Adhyaksa GWP. Understanding losses in halide perovskite thin films: Van der Waals- Zeeman Institute (WZI); 2018.
[14] Jia X, Hu Z, Zhu Y, Weng T, Wang J, Zhang J, et al. Facile synthesis of organic–inorganic hybrid perovskite $CH_3NH_3PbI_3$ microcrystals. Journal of Alloys and Compounds. 2017;725:270-4.
[15] Zhang F, Zhu K. Additive Engineering for Efficient and Stable Perovskite Solar Cells. Advanced Energy Materials. 2019;10(13):1902579.
[16] Mazloum-Ardakani M, Arazi R. The investigation on different light harvesting layers and their sufficient effect on the photovoltaic characteristics in dye sensitized solar cell. Nanochemistry Research. 2017;2(1):20-8.
[17] Hou M, Zhang H, Wang Z, Xia Y, Chen Y, Huang W. Enhancing Efficiency and Stability of Perovskite Solar Cells via a Self-Assembled Dopamine Interfacial Layer. ACS Applied Materials & Interfaces. 2018;10(36):30607-13.
[18] Zhang J, Yu H. Multifunctional dopamine-assisted preparation of efficient and stable perovskite solar cells. Journal of Energy Chemistry. 2021;54:291-300.
[19] Iram S, Imran M, Kanwal F, Latif S, Iqbal Z. Bismuth and lead based metal organic frameworks: morphological, luminescence and Brunauer-Emmett-Teller (BET) studies. Materials Science-Poland. 2020;38(1):132-7.
[20] E Z. Development and Application of Novel Optoelectronic Materials for Photodetectors and Solar Cells: University of Washington; 2020.
[21] Mabrouk S, Dubey A, Zhang W, Adhikari N, Bahrami B, Hasan MN, et al. Increased Efficiency for Perovskite Photovoltaics via Doping the PbI_2 Layer. The Journal of Physical Chemistry C. 2016;120(43):24577-82.
[22] Li M, Li B, Cao G, Tian J. Monolithic $MAPbI_3$ films for high-efficiency solar cells via coordination and a heat assisted process. J Mater Chem A. 2017;5(40):21313-9.
[23] Li J, Dong X, Liu T, Liu H, Wang S, Li X. Electronic Coordination Effect of the Regulator on Perovskite Crystal Growth and Its High-Performance Solar Cells. ACS Applied Materials & Interfaces. 2020;12(17):19439-46.
[24] Xue J, Wang R, Wang K-L, Wang Z-K, Yavuz I, Wang Y, et al. Crystalline Liquid-like Behavior: Surface-Induced Secondary Grain Growth of Photovoltaic Perovskite Thin Film. Journal of the American Chemical Society. 2019;141(35):13948-53.
[25] Tavakoli MM, Yadav P, Prochowicz D, Sponseller M, Osherov A, Bulović V, et al. Controllable Perovskite Crystallization via Antisolvent Technique Using Chloride Additives for Highly Efficient Planar Perovskite Solar Cells. Advanced Energy Materials. 2019;9(17):1803587.

CC BY